Polycationic Redox-Active Cyclophanes with Integrated Electron-Rich Diboron Units

Erik Filbeck,[a] Anna Widera,[a] Elisabeth Kaifer,[a] and Hans-Jörg Himmel*[a]

Abstract: Cationic cyclophanes are widely used in a variety of applications in supramolecular chemistry and materials science. In this work the authors systematically study the integration of electron-rich diboron units with B^{II} atoms into polycationic cyclophanes with viologen-like electron-acceptor units. They also report a first hexacationic cage-compound in which three diboron units connect two tris(4-pyridyl)triazine acceptor units. Moreover, di- and tetracationic open-structure compounds, in which one diboron unit connects two bispyridyl groups, were synthesized and the properties compared to those of the corresponding closed structures (cyclophanes). The combination of diboron electron-donor units and bi- or oligopyridyl electron-acceptor units leads to intriguing optical and redox properties.

Introduction

Organic macrocycles and rings are intensively studied, since they are interesting for a variety of applications in supramolecular chemistry and materials science. Especially, viologen-like linkers are used in a number of polycationic cyclophanes.[1] As example, Figure 1 displays the Lewis structure of the archeotypical tetracation cyclobis(paraquat-*p*-phenylene) ($CBPQT^{4+}$), synthesized already in 1988 independently by Stoddart and Hünig,[2,3] and used for host-guest chemistry and as key component in molecular shuttles, switches and machines.[4] The electron-poor viologen units are versatile electron-acceptors, enabling the incorporation of small electron-donor molecules such as hydroquinone,[5] and producing intriguing redox properties. A variety of further polycationic cyclophanes with viologen-like units were synthesized,[4] with variable diameters (see, for example, the boxlike cyclobis (paraquat-*p*-biphenylene) tetraction ($CBPQTBP^{4+}$) in Figure 1 comprising two 4,4′-phenylene-linked "extended" bipyridinium units,[6] and/or integrated functional groups, as for example the tetrazine units in the recently reported "TetrazineBox").[7] Very recently, the first cyclotris(paraquat-*p*-phenylenes) were synthesized.[8] Jäkle et al. synthesized several boracyclophanes with interesting optical and redox properties.[9–14] One example is sketched in Figure 1. In these compounds, the B^{III} atoms are Lewis-acidic sites and act as electron-acceptors.[10]

The aim of our research in this field is the integration of diboron electron-donor units into polycationic cyclophanes with viologen-like electron acceptor units.[15] A suitable compound for the synthesis of electron-rich diboron building blocks is the ditriflato-diborane $B_2(hpp)_2(OTf)_2$ (**1**) with hpp = 1,3,4,6,7,8-hexahydro-2*H*-pyrimido[1,2-α]pyrimidinate (Scheme 1), exhibiting two strongly electron-donating bridging guanidinate substituents and two triflato groups that could easily be substituted by neutral Lewis bases.[16–19] The low oxidation state of the boron atoms (B^{II}) and the guanidinate substituents turn diborane **1** into an electron-donor (in difference to most other known boron compounds). The hypothetical dicationic diboron building block arising from abstraction of both triflato substituents by a Lewis acid ($AlCl_3$ or $GaCl_3$) precipitates from solution as insoluble, bright-red and fluorescent dimer with rhomboid B_4 core and (4c,4e) bonding (two closed B–B–B (3c,2e) bonds that share an edge).[16] Its one-electron reduction produces a soluble radical trication (Scheme 1).[20,21,22]

On the other hand, the addition of 4,4′-bipyridine (L1) or 1,2-di(4-pyridyl)ethylene (L2) to a solution of **1** leads to the formation of tetracationic cyclophanes $[\{B_2(hpp)_2\}_2(L1)_2]^{4+}$ and $[\{B_2(hpp)_2\}_2(L2)_2]^{4+}$ (Scheme 2).[15] The substitution of the triflato groups by the neutral bipyridine is likely to occur via an S_N1 reaction mechanism, initiated by triflate dissociation (see Figure 2). The resulting two unprecedented novel polycationic cyclophanes, combining for the first time bispyridyl electron-acceptor units with diboron electron-donor units, were structurally characterized in the solid-state. The diboron units with their tetracoordinate (sp^3-hybridized) B^{II} atoms act as ethylene-analogue bridges, but in difference to ethylene linkers they are redox-active[23] by virtue of the strong electron-donating character of the two bicyclic guanidinate bridges and the low boron oxidation state (B^{II}).

The two intact B–B bonds enforce quite close proximity of the two viologen-like organic π-systems. In difference to $CBPQT^{4+}$ and related polycationic organic cyclophanes, the cavities in $[\{B_2(hpp)_2\}_2(L1)_2]^{4+}$ and $[\{B_2(hpp)_2\}_2(L2)_2]^{4+}$ are too

[a] *E. Filbeck, Dr. A. Widera, Dr. E. Kaifer, Prof. H.-J. Himmel*
Institute of Inorganic Chemistry
Ruprecht-Karls University of Heidelberg
Im Neuenheimer Feld 270, 69120 Heidelberg (Germany)
E-mail: hans-jorg.himmel@aci.uni-heidelberg.de

Supporting information for this article is available on the WWW under https://doi.org/10.1002/chem.202102656

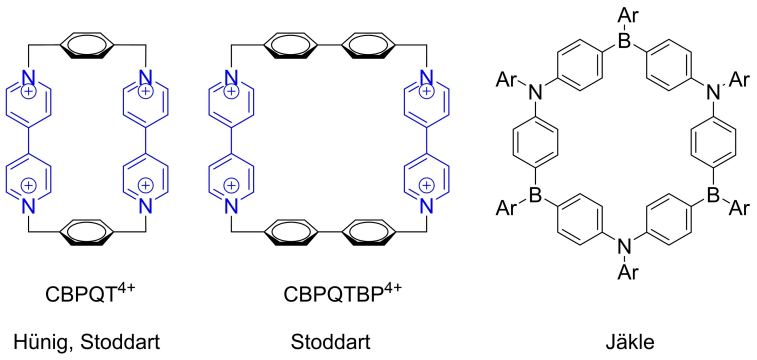

Figure 1. Lewis structures of two typical tetracationic viologen cyclophanes, illustrating the possibility to tune the ring size, and of a boracyclophane.

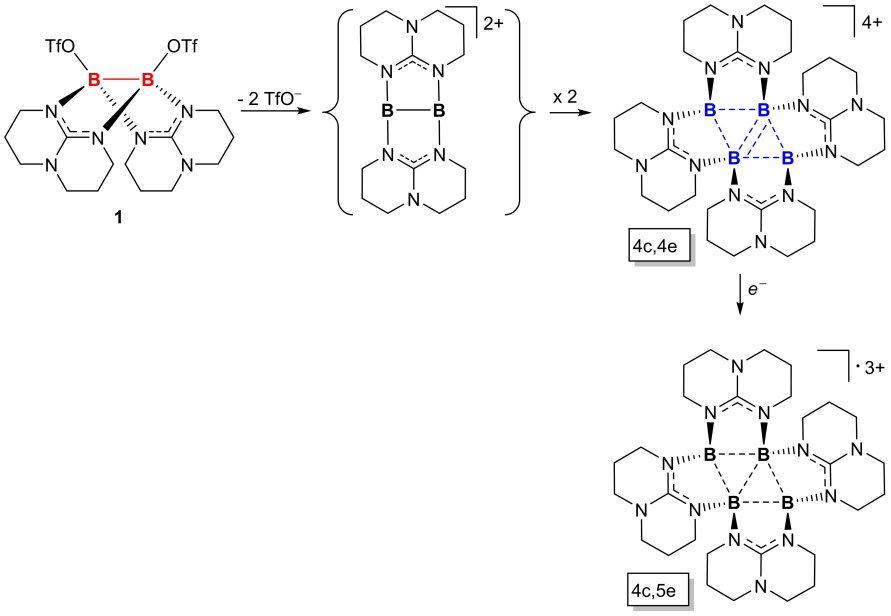

Scheme 1. The ditriflato-diborane **1**, an excellent precursor for dicationic diboron building blocks for integration in polycationic cyclophanes with viologen-like electron acceptor units. In the absence of a Lewis base, the abstraction of the two triflato groups with $AlCl_3$ or $GaCl_3$ induces dimerization to the tetraboron tetracation $[B_4(hpp)_4]^{4+}$. The tetracation could be reduced to the radical trication, with retention of the rhomboid B_4 core. In the course of dimerization, the diboron unit changes from an electron-donor (highlighted in red) to an electron acceptor (highlighted in blue).

small for introduction of an electron-rich guest molecule, but the compounds show intriguing optical and redox properties. They share a typical overall electron-acceptor property with Stoddart's cyclophanes, but are in addition amenable to intramolecular electron (charge) transfer. This is demonstrated by the outcome of the reaction of **1** with the stronger electron-acceptor pyrazine (Scheme 2).[15] Here, the formation of a tetracationic ring is accompanied with electron-transfer from the diboron to the pyrazine units. In the course of this electron transfer, the two B–B bonds are cleaved and a macrocyclic ring compound with four B^{III} atoms is formed. Addition of two triflato substituents ensures the preservation of two four-coordinate boron atoms. To highlight the presence of electron-donor and electron-acceptor units, we use throughout this paper blue colour for the electron-accepting viologen-like section of the cyclophanes, and red colour for the electron-donating diboron units.

In this work, we report a first systematic study of this novel compound class. A variety of cyclophanes with different rigid or flexible bis- and trispyridyl groups (see Figure 2) was synthesized to address a number of important issues. First, it is analysed how the optical and redox properties alter with the size of the viologen-like units. Moreover, open-structure compounds with two bispyridyl units connected by only one diboron unit were synthesized to compare their optical and redox properties with those of the corresponding closed forms (cyclophanes). Finally, we report the first hexacationic cage compound with three diboron units, paving the way to larger redox-active macrocycles with integrated diboron electron-donor units and oligopyridyl electron-acceptor units.

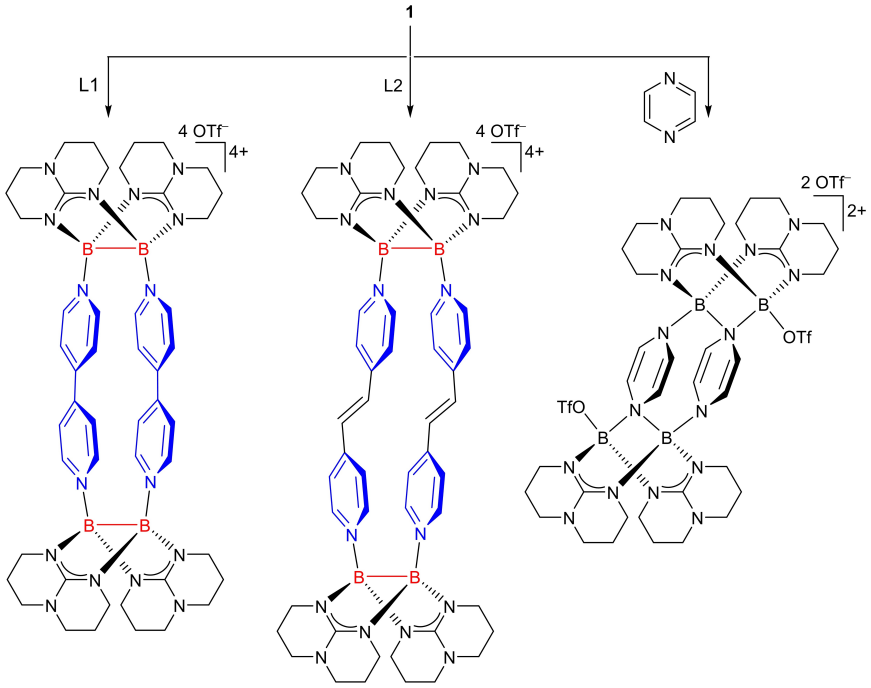

Scheme 2. Reactions of the ditriflato-diborane **1** with L1/L2, leading to the first polycationic cyclophanes in which bispyridyl acceptor units are combined with diboron electron-donor units. In the case of reaction between **1** and pyrazine, ring formation is accompanied by electron transfer from the diboron to the pyrazine units.

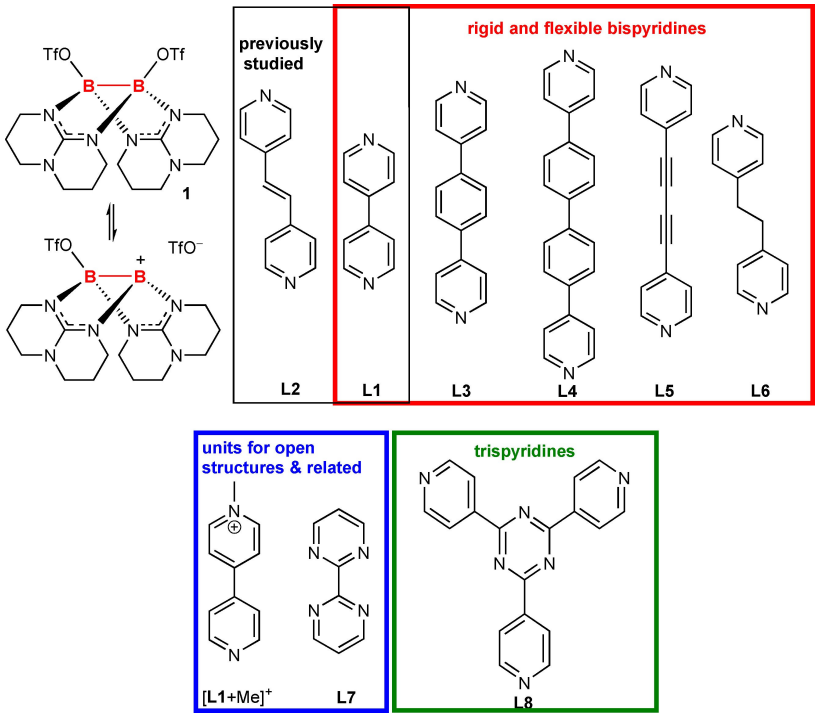

Figure 2. Equilibrium showing the formation of free diboron cations by triflate dissociation from diborane **1**, as well as Lewis structures and labels (L1 - L8) of the linker units for the construction of cyclophanes and related structures used in this work, sorted by their specific features.

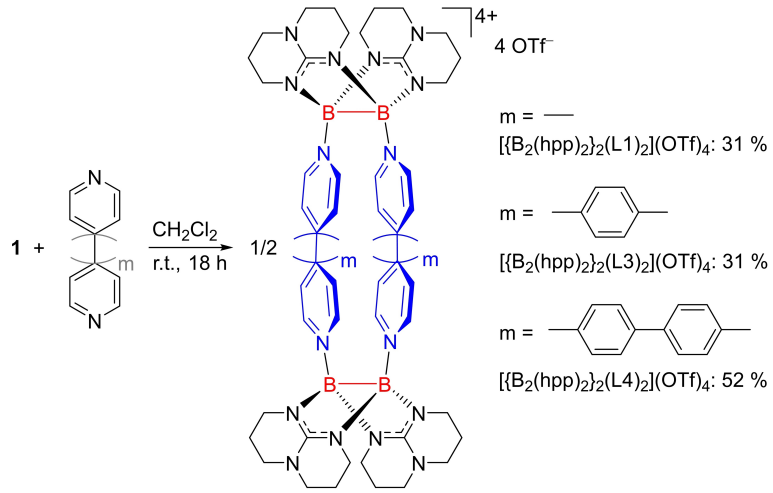

Scheme 3. Synthesis of tetracationic tetraboron cyclophanes with different sizes of the bispyridyl units.

Results and Discussion

Rigid bispyridines

The optical and redox properties of $[\{B_2(hpp)_2\}_2(L1)_2]^{4+}$ and $[\{B_2(hpp)_2\}_2(L2)_2]^{4+}$ are very different to those of free L1 and L2, respectively, and should respond specifically to an extension of the viologen-like units (see bispyridines in the red box). Therefore, we aimed at the preparation of new extended cyclophanes by using the "extended" bispyridines L3 and L4 (Figure 2). Indeed, reaction of **1** with one equivalent of either L3 or L4 in CH_2Cl_2 at room temperature yielded the new tetracationic tetraboron cyclophanes $[\{B_2(hpp)_2\}_2(L3)_2]^{4+}$ and $[\{B_2(hpp)_2\}_2(L4)_2]^{4+}$ (Scheme 3). The salt $[\{B_2(hpp)_2\}_2(L3)_2](OTf)_4$ was obtained in the form of yellow crystals by layering a solution in CH_3CN with Et_2O, and the salt $[\{B_2(hpp)_2\}_2(L4)_2](OTf)_4$ precipitated as a pale-yellow solid from the CH_2Cl_2 reaction mixture. Unfortunately, only for $[\{B_2(hpp)_2\}_2(L1)_2](OTf)_4$ and $[\{B_2(hpp)_2\}_2(L3)_2](OTf)_4$ crystals suitable for a structural analysis were obtained,[15] but all analytic data clearly show that the compound with L4 adopts a similar cyclophane structure. In the ESI^+ spectra, measured for solutions of the compounds in CH_3CN, peaks associated with the tetracationic cyclophane unit and a varying number of triflate counter ions (e.g. m/z = 679.2764 and 1507.5053 for $[\{B_2(hpp)_2\}_2(L3)_2(OTf)_2]^{2+}$ and $[\{B_2(hpp)_2\}_2(L3)_2(OTf)_3]^+$ respectively; m/z = 755.3075 and 1659.5750 for $[\{B_2(hpp)_2\}_2(L4)_2(OTf)_2]^{2+}$ and $[\{B_2(hpp)_2\}_2(L4)_2(OTf)_3]^+$, respectively) indicate that the cyclophanes are stable in solution. Also, the NMR spectra indicate the presence of intact cyclophane units. In Figure 3, the ^1H NMR (only aromatic region from $\delta = 9.00$ to 7.00 ppm), ^{11}B and ^{19}F NMR spectra of $[\{B_2(hpp)_2\}_2(L3)_2](OTf)_4$ are compared to the spectra obtained for the reactants. The ^{11}B NMR spectrum contains a single signal for all boron atoms at $\delta = 4.19$ ppm, being slightly shifted with respect to the diborane reactant $B_2(hpp)_2(OTf)_2$ ($\delta = 4.53$ ppm). Three signals, two doublets and a singlet, appear in the aromatic region of the ^1H NMR spectrum

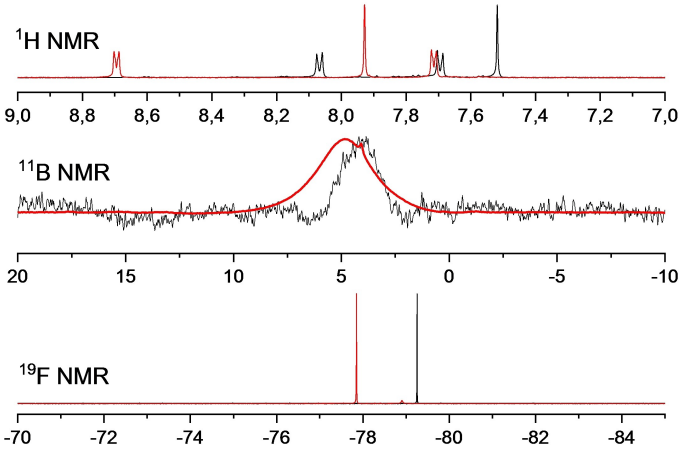

Figure 3. ^1H NMR spectra of $[\{B_2(hpp)_2\}_2(L3)_2](OTf)_4$ (black) and L3 (red) in CH_3CN; ^{11}B NMR and ^{19}F NMR spectra of $[\{B_2(hpp)_2\}_2(L3)_2](OTf)_4$ (black) and **1** (red) in CH_3CN.

of $[\{B_2(hpp)_2\}_2(L3)_2]^{4+}$, in line with the presence of two chemically equivalent bispyridine units L3 (Figure 3). Their chemical shifts are significantly different from those of the free bispyridine L3. Moreover, the ^{19}F NMR spectrum shows the sole presence of free triflate ($\delta = -79.21$ ppm). Hence, the triflate groups are completely substituted by bispyridine (L3). Similar results were obtained for $[\{B_2(hpp)_2\}_2(L4)_2](OTf)_4$ (see Supporting Information).

In the case of reaction between **1** and L1, we observed an immediate color change from colorless to green; an EPR spectrum recorded for the solution at this stage indicated the presence of radical intermediates.[15] Hence, the reaction seems to be initiated by electron transfer from the electron-rich diborane **1** to the electron-acceptor L1. After some time, the reaction mixture turned red and formation of the diamagnetic cyclophane product $[\{B_2(hpp)_2\}_2(L1)_2]^{4+}$ was completed. On the other hand, no comparable observations were made for the reaction between **1** and L3 or L4; radical intermediates arising

from electron transfer are not formed in significant amount. This result is in line with the lower electron-acceptor character of L3 and L4 in comparison with L1.

The extension of the viologen-like units is accompanied by a marked decrease of the solubility of the resulting cyclophanes. While $[\{B_2(hpp)_2\}_2(L1)_2](OTf)_4$ still displays a decent solubility in CH_2Cl_2 and CH_3CN, $[\{B_2(hpp)_2\}_2(L4)_2](OTf)_4$ is barely soluble in CH_2Cl_2 and only moderately soluble in CH_3CN. The UV-vis spectroscopic and cyclic voltammetry measurements of the new cyclophanes were therefore carried out in CH_3CN solutions.

In Figure 4, the UV-vis spectra are compared, and the embedded photo compares the colours of the different cyclophanes. $[\{B_2(hpp)_2\}_2(L1)_2](OTf)_4$ shows a broad absorption centered at 397 nm, being responsible for its intense orange colour, and a sharper one at 251 nm. For comparison, the UV-vis spectrum of free L1 contains a single strong band in the UV region at 238 nm, the visible region is free of absorptions. The low-energy band around 397 nm in the spectrum of $[\{B_2(hpp)_2\}_2(L1)_2](OTf)_4$ could be assigned to a charge-transfer transition from the electron-rich diboron units to the pyridinium acceptor units (see below). Hence, this band is typical for this novel family of donor-acceptor cyclophanes. The UV-vis spectrum of $[\{B_2(hpp)_2\}_2(L3)_2](OTf)_4$ also displays two absorptions, with maxima at 299 and 364 nm. The low-energy charge-transfer absorption is slightly blue-shifted by 34 nm with respect to the cyclophane with L1, in line with the higher LUMO energy of L3 compared with L1. On the other hand, the band in the UV region is slightly red-shifted by 48 nm. For free L3, a band at 278 nm is observed, being red-shifted compared to free L1 by 40 nm. This band could be assigned to an electronic excitation localized on the bispyridyl π-system. As a result, the energy separation between the two bands decreases. In $[\{B_2(hpp)_2\}_2(L4)_2](OTf)_4$, the energy difference between the two bands further decreases; only one absorption maximum at 333 nm is visible, and the charge-transfer transition appears as a shoulder at about 360 nm. The UV-vis spectra thus show a trend of the charge-transfer band towards higher energy with increasing lengths of the bispyridyl units, being in line with the trend of increasing LUMO energy of the free bispyridines.

To obtain additional information, the cyclophanes $[\{B_2(hpp)_2\}_2(L1)_2]^{4+}$ and $[\{B_2(hpp)_2\}_2(L3)_2]^{4+}$ were calculated by DFT methods (B3LYP + D3/def2-TZVP). The structure calculated for $[\{B_2(hpp)_2\}_2(L1)_2]^{4+}$ was found to be in pleasing agreement with the experimental solid-state structure.[15] The calculated B–B bond length amounts to 1.765 Å (exp. 1.728(8)/1.724(8) Å) and the distance between the two dipyridyl units (C atoms in position 4 of the pyridyl rings) to 3.927 Å (exp. 4.0266(1)/4.0335(1) Å). The calculated structure for $[\{B_2(hpp)_2\}_2(L3)_2]^{4+}$ is also in good agreement with the experimentally determined structure from XRD (see Supporting Information),[24] with a B–B bond length of 1.747 Å (exp. 1.7248(2) Å) and a distance between the C atoms in position 4 of the pyridyl rings of 4.010 Å (exp. 3.8069(4) Å). Figure 5 displays isodensity plots for the HOMO and LUMO of the two tetracations $[\{B_2(hpp)_2\}_2(L3)_2]^{4+}$ and $[\{B_2(hpp)_2\}_2(L1)_2]^{4+}$. As expected, the HOMO is located on the diboron units and the LUMO on the bispyridyl units. The HOMO-LUMO gap increases from 2.6 eV in $[\{B_2(hpp)_2\}_2(L1)_2]^{4+}$ to 3.1 eV in $[\{B_2(hpp)_2\}_2(L3)_2]^{4+}$, in line with the blue shift of the charge-transfer band in the UV-vis spectra.

The curves obtained from cyclic voltammetry measurements are reproduced in Figure 6, and the measured potentials are compiled in Table 1. Please note that the CV curve of $[\{B_2(hpp)_2\}_2(L1)_2](OTf)_4$ in CH_2Cl_2 solution, showing "better-resolved" redox waves, was published previously.[15] However,

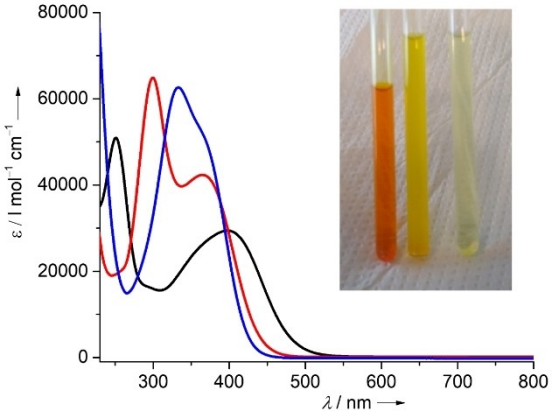

Figure 4. UV-vis spectra of $[\{B_2(hpp)_2\}_2(L1)_2](OTf)_4$ (black curve) $[\{B_2(hpp)_2\}_2(L3)_2](OTf)_4$ (red curve) and $[\{B_2(hpp)_2\}_2(L4)_2](OTf)_4$ (blue curve) in CH_3CN. The embedded photo compares the colour of CH_3CN solutions of $[\{B_2(hpp)_2\}_2(L1)_2](OTf)_4$, $[\{B_2(hpp)_2\}_2(L3)_2](OTf)_4$ and $[\{B_2(hpp)_2\}_2(L4)_2](OTf)_4$ (from left to right).

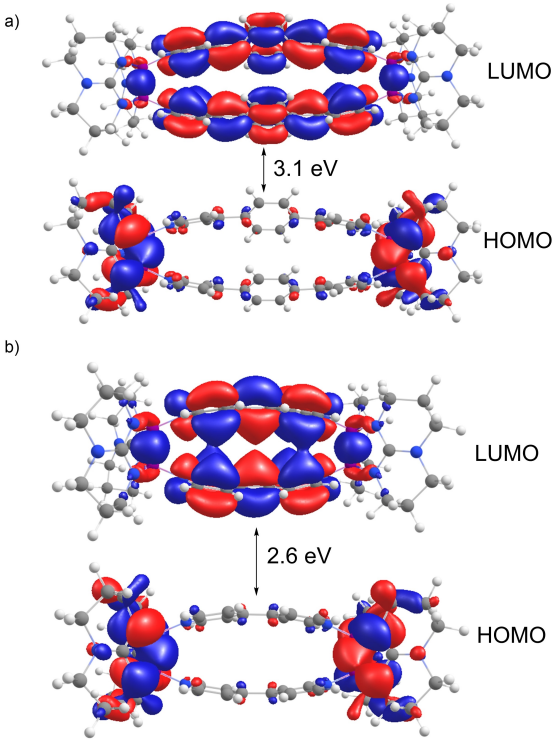

Figure 5. Illustration of the isodensity surfaces (isovalue = 0.02) for the HOMO und LUMO of a) $[\{B_2(hpp)_2\}_2(L3)_2]^{4+}$ and b) $[\{B_2(hpp)_2\}_2(L1)_2]^{4+}$ according to B3LYP + D3/def2-TZVP calculations.

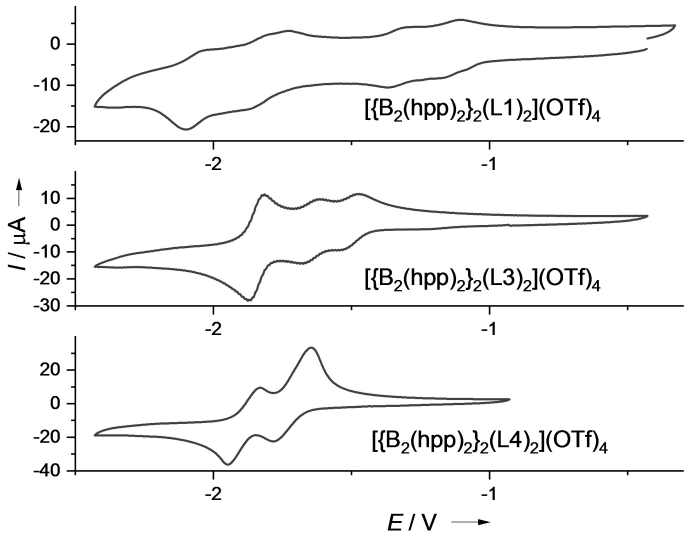

Figure 6. Cyclic voltammograms of $[\{B_2(hpp)_2\}_2(L1)_2](OTf)_4$, $[\{B_2(hpp)_2\}_2(L3)_2](OTf)_4$ and $[\{B_2(hpp)_2\}_2(L4)_2](OTf)_4$ (all measured in CH_3CN at 298 K with a scan rate of 100 mV s^{-1} (glassy carbon working-electrode, Pt counter-electrode, Ag/AgCl reference electrode) with 0.1 M nBu$_4$NPF$_6$ as supporting electrolyte). Potentials are given vs. the ferrocenium/ferrocene (Fc^+/Fc) redox couple.

since the solubility in CH_2Cl_2 is too low for the cyclophane with L4 units, we show here the CV curve in CH_3CN. As expected from the trend in the electron-acceptor strength of the bispyridines, the redox potentials of the three cyclophanes vary. Since both bispyridyl units could be reduced, two-electron redox processes are expected to show in the cyclic voltammograms if the two units are not electronically coupled. On the other hand, the presence of electronic coupling between the two units leads to one-electron redox processes at different potential. A two-electron redox process at $E_{1/2} = -1.72$ V, assigned to the redox couple $[\{B_2(hpp)_2\}_2(L4)_2]^{4+}$/$[\{B_2(hpp)_2\}_2(L4)_2]^{2+}$, is observed for the cyclophane with L4 bispyridyl groups. Hence, the cyclophane $[\{B_2(hpp)_2\}_2(L4)_2](OTf)_4$ exhibits the lowest reduction potential and therefore is the weakest electron acceptor. The redox potential clearly decreases with increasing size of the viologen-like linker. This result is in full agreement with the UV-vis results and also with the trend of the irreversible reduction potentials of the free bispyridines. Two one-electron redox events at different potential occur for the cyclophanes with L1 and L3, $[\{B_2(hpp)_2\}_2(L1)_2](OTf)_4$ and $[\{B_2(hpp)_2\}_2(L3)_2](OTf)_4$; $E_{1/2}$ values of −1.14 V for the redox couple $[\{B_2(hpp)_2\}_2(L1)_2]^{4+}$/$[\{B_2(hpp)_2\}_2(L1)_2]^{3+}$ and $E_{1/2} = -1.51$ V for the redox couple $[\{B_2(hpp)_2\}_2(L3)_2]^{4+}$/$[\{B_2(hpp)_2\}_2(L3)_2]^{3+}$ were measured. (Please note that the assignment of the waves to one- or two-electron redox events is motivated by the relative intensities of the waves in the same CV curve.). Hence, the two bispyridyl groups are electronically coupled in the cyclophanes with L1 and L3 units, but not in the cyclophane with L4 units.

We also tested the possibility to construct cyclophanes with bispyridines in which the two pyridyl units are connected by the rigid butadiyne unit (linker di(4-pyridyl)butadiyne, L5) as well as a more flexible ethane unit (linker 1,2-di(4-pyridyl) ethane, L6). Reaction between **1** and L5 in a CH_2Cl_2 solution resulted in a dark reaction mixture, from which a few crystals of the salt $[\{B_2(hpp)_2\}_2(L5)_2](OTf)_4$ precipitated. Fortunately, these crystals were suitable for a structural analysis by SCXRD. The resulting solid-state structure of the tetracationic tetraboron cyclophane $[\{B_2(hpp)_2\}_2(L5)_2]^{4+}$ is visualized in Figure 7a.[24] The B–B bond length of 1.7390(3) Å indicates the presence of intact B–B bonds. The B–N bonds connecting the L5 units with the diboron units measure 1.5807(3) and 1.5804(3) Å. The separation between the two L5 units in the new polycationic cyclophane is 3.8496(6) Å for the C atoms in 4-position of the pyridyl groups (see Figure 7a). The compound turned out to be extremely light-sensitive, and had to be kept in the dark to avoid light-induced decomposition, leading to so far unidentified products. It was not possible to obtain a larger amount of this compound in pure form, prohibiting further analysis.

Reaction between diborane **1** and 1,2-di(4-pyridyl)ethane (L6) gave $[\{B_2(hpp)_2\}_2(L6)_2](OTf)_4$. The flexible structure leads to a slight increase in the separation of the two bispyridine units (Figure 7b).[24] Hence, the distances between the carbon atoms in 4-position of the pyridyl groups is 4.5952(5) Å in $[\{B_2(hpp)_2\}_2(L6)_2]^{4+}$. The B–B bonds are 1.7155(2) Å long, and the B–N bond distances connecting the diboron units with the L6 units measure 1.5844(1) and 1.5912(2) Å. As expected, charge-transfer bands are absent in the UV-vis spectrum of $[\{B_2(hpp)_2\}_2(L6)_2](OTf)_4$ (see Supporting Information); the visible region is free of absorptions. Additional experiments with 1,2-di(4-pyridyl)propane produced product mixtures from which it was not possible to isolate a pure compound in larger yield. Nevertheless, a small amount of crystals was obtained; a preliminary structural analysis with XRD revealed the presence of a cyclic compound with a $[B_2(hpp)_2]^{2+}$ unit, to which one 1,2-di(4-pyridyl)propane is bound by two B–N bonds to both pyridyl groups (see Supporting Information). This result indicates the limits for the synthesis of cyclophane boranes with flexible linkers.

Table 1. Potentials (in V, given vs. Fc^+/Fc) measured in CH_3CN solution.

Compound	$E_{1/2}(1)/E_{red}(1)$	$E_{1/2}(2)/E_{red}(2)$	$E_{1/2}(3)/E_{red}(3)$	$E_{1/2}(4)/E_{red}(4)$
$[\{B_2(hpp)_2\}_2(L1)_2](OTf)_4$[a]	−1.14/−1.18	−1.21/−1.38	−1.80/−1.87	−2.06/−2.10
$[\{B_2(hpp)_2\}_2(L3)_2](OTf)_4$	−1.51/−1.53	−1.64/−1.68	−1.84/−1.88	−1.84/−1.88
$[\{B_2(hpp)_2\}_2(L4)_2](OTf)_4$	−1.72/−1.78	−1.72/−1.78	−1.89/−1.95	−1.89/−1.95

[a] Broad waves.

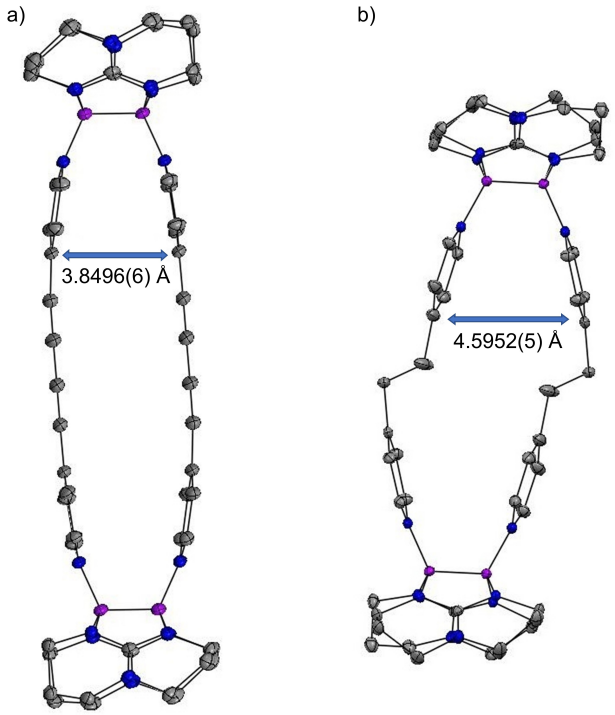

Figure 7. Illustration of the solid-state structure of the tetracationic cyclophane $[\{B_2(hpp)_2\}_2(L5)_2]^{4+}$ (a) and $[\{B_2(hpp)_2\}_2(L6)_2]^{4+}$ in crystals of their triflate salts. Triflate counterions and hydrogen atoms are omitted. Displacement ellipsoids drawn at the 50% probability level. Colour code: B purple, C grey, N blue.

Open-structure compounds

Compounds with an open structure, in which two viologen-like units are connected only by one diboron unit, are of interest for a variety of reasons. First, the comparison of their structures as well as redox and optical properties with those of the corresponding closed structures (cyclophanes) should be informative. Then, they eventually might provide access to polycationic cyclophanes with one diboron unit and a different (organic) unit of variable size and properties at the other end of the macrocyclic ring. Herein, we concentrate on the first point, the comparison of the redox and optical properties.

Indeed, it was possible to synthesize the open-structure compound $[B_2(hpp)_2(L1)_2](OTf)_2$ by reacting the ditriflato-diborane **1** with an excess (five equivalents) of L1 in CH_2Cl_2 at room temperature (Scheme 4a). The ESI^+ mass spectrometric analysis found a peak of maximal intensity at m/z = 759.3140 due to $[B_2(hpp)_2(L1)_2(OTf)]^+$ (see Supporting Information), indicating the presence of the open-structure dication in solution. In the ^{11}B NMR spectrum (see Supporting Information), a signal appeared at $\delta = 3.57$ ppm, shifted slightly from the value of $\delta =$ 4.53 ppm in **1**. The ^1H NMR spectrum indicates that both bispyridyl (L1) groups are chemically equivalent (four signals in the aromatic region). Interestingly, the reaction mixture first turned from colourless to deep-green. At the end of the reaction period of 18 h, the solution adopted an orange colour. Red crystals of the final product $[B_2(hpp)_2(L1)_2](OTf)_2$ suitable for structural analysis by SCXRD were grown from a CH_2Cl_2 solution layered with *n*-pentane. The analogy to the observations made for the reaction in a 1:1 ratio leading to the closed structure $[\{B_2(hpp)_2\}_2(L1)_2](OTf)_4$ (see discussion above and Ref. [15]) indicates that the same radical intermediate is formed in both reactions. This intermediate might be the 1:1 complex $[B_2(hpp)_2(L1)(OTf)]OTf$ in which one of the triflato groups is substituted by L1, and an electron transferred from the electron-rich diboron unit to L1. Scheme 4b illustrates possible pathways to this intermediate. Obviously, substitution of the first triflate from the neutral diborane $B_2(hpp)_2(OTf)_2$ by a neutral bipyridine in an S_N1 mechanism should be faster than substitution of the second one, since elimination of the second triflate ion from the $[B_2(hpp)_2(L1)(OTf)]^+$ intermediate stage is hindered by the opposite charges. The electron transfer enables addition of a second bispyridine prior to triflate elimination. Another possibility is that the produced $[B_2(hpp)_2(L1)_2]^{2+}$ is first reduced to a radical monocation by unconsumed diborane molecules **1**, before it is re-oxidized in the course of the reaction to allow further product formation. However, further addition of diborane **1** to a solution of the product did not lead to a colour change. Therefore, this alternative is not plausible.

We were also able to prepare the open-structure compound $[B_2(hpp)_2(L2)_2](OTf)_2$ by reacting diborane **1** with five equivalents of L2 in CH_2Cl_2 (Scheme 4a). Again, only one signal is observed in the ^{11}B NMR spectrum, located at $\delta = 3.28$ ppm. The compound was isolated in 28% yield in the form of yellow crystals by layering a solution of CH_2Cl_2 with *n*-pentane. An additional experiment, in which the possibility for a photo-induced [2+2] cycloaddition reaction between the two double bonds in $[B_2(hpp)_2(L2)_2]^{2+}$ was tested by irradiating a solution of the compound at different wavelengths, gave no clear results.[25–27]

Finally, the salt $[B_2(hpp)_2(L1+Me)_2](OTf)_2I_2$ was obtained in 76% isolated yield by reacting diborane **1** with two equivalents of (L1+Me)I in CH_2Cl_2 solution. The ^{11}B NMR spectrum shows a single signal at $\delta = 3.70$ ppm. The ^1H NMR spectrum contains four signals in the aromatic region (see Supporting Information), indicating the equivalence of the two units of (L1+Me). The ^{19}F NMR spectrum confirms the sole presence of solvated triflate (OTf^-) ions in solution; all boron-bound triflate groups were substituted. During the reaction, an immediate color change to cyan-green was observed. In the EPR spectrum recorded of the reaction mixture at this stage, a signal at g = 2.0035 appeared, indicating the formation of radical intermediates (see Supporting Information for details). On the basis of the considerations and experiments made for related reactions (see discussion above), we postulate this intermediate to be $[B_2(hpp)_2(L1+Me)(OTf)]^{2+}$. The final product $[B_2(hpp)_2(L1+Me)_2](OTf)_2I_2$ precipitated as pale-yellow solid from the green reaction mixture (see photo imbedded in Scheme 4a).

The solid-state structure of the dication $[B_2(hpp)_2(L1)_2]^{2+}$ from an SCXRD analysis is visualized in Figure 8.[24] The compound exhibits an intact B–B bond with a length of 1.7005(1) Å. The two B–N bonds connecting the two units of L1 with the diboron unit measure 1.5864(1) and 1.5816(1) Å. The distance between the two equivalent units of L1 widens with

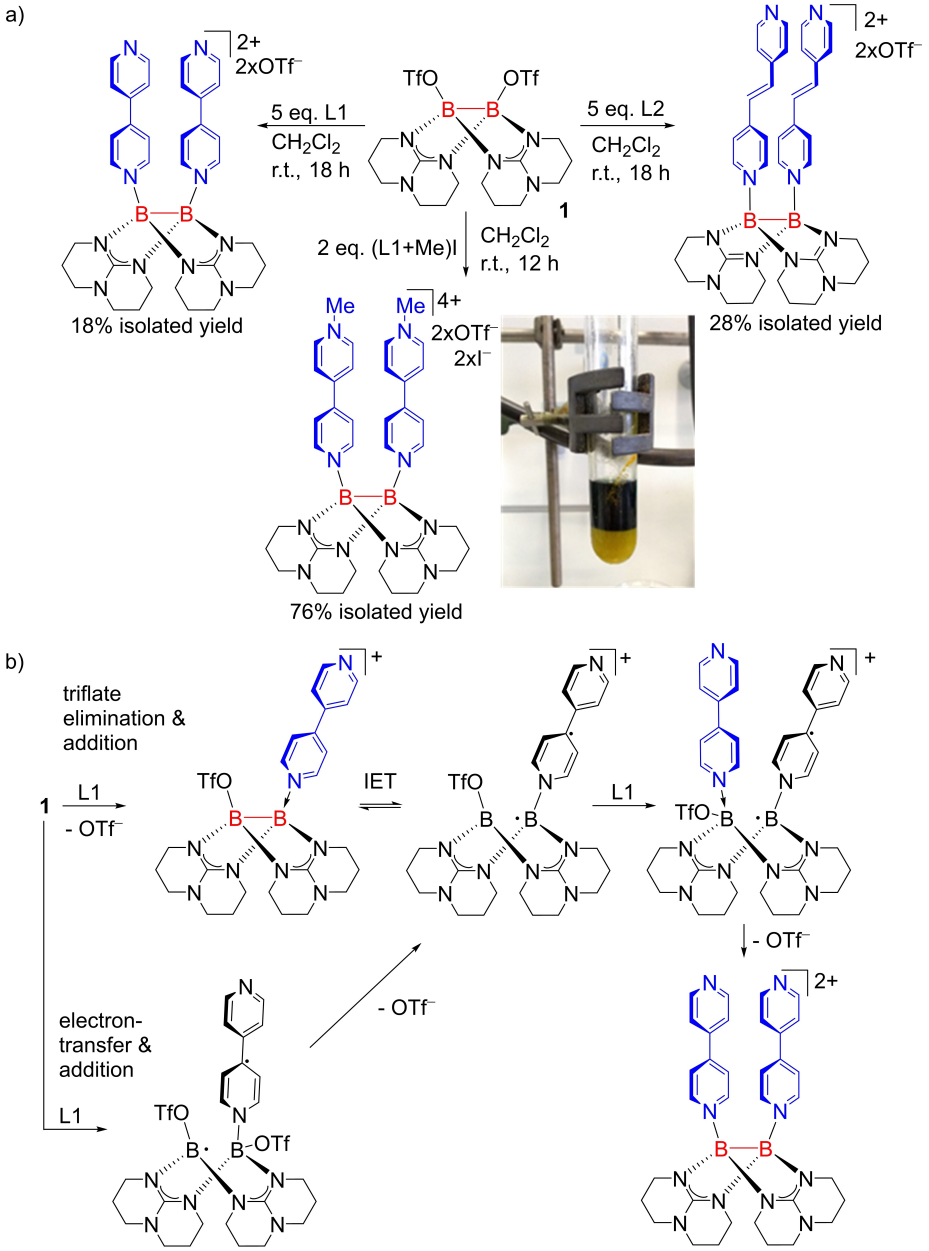

Scheme 4. a) Synthesis of the open-structure compounds $[B_2(hpp)_2(L1)_2]^{2+}$, $[B_2(hpp)_2(L1+Me)_2]^{4+}$ and $[B_2(hpp)_2(L2)_2]^{2+}$. Photo of a CH_2Cl_2 solution of **1** with two equivalents of (L1 + Me)I after 24 h reaction time showing the precipitated salt $[B_2(hpp)_2(L1+Me)_2](OTf)_2I_2$ and the remaining green solution. b) Possible mechanisms for the reaction of **1** with two equivalents of L1 leading to $[B_2(hpp)_2(L1)_2]^{2+}$ (IET denotes intramolecular electron transfer).

increasing distance to the diboron unit. Hence, the two N atoms directly bound to B atoms are separated by only 3.1450(3) Å, but the two N atoms at the other end of the bipyridine unit are already 8.4507(7) Å apart. The distance between the carbon atoms in 4-position of the pyridyl groups measures 5.1278(4) Å (Figure 8). The two B–B–N angles (N being one of the pyridine-nitrogen atoms directly bound to boron) measure 115.6° and 118.6°.

To complement our analysis, we calculated the tetracation $[B_2(hpp)_2(L1+Me)_2]^{4+}$ by DFT methods (B3LYP/def2-TZVP). Figure 9a sketches the resulting energy minimum structure. Since the organic units $(L1+Me)^+$ carry an additional charge, the two equally-charged (L1 + Me) units sense a larger columbic repulsion than in $[B_2(hpp)_2(L1)_2]^{2+}$. While the two nitrogen atoms directly bound to the B atoms are separated by 3.631 Å, the methyl-bound nitrogen atoms at the other side of the organic linker units are already separated by 13.569 Å. With 7.346 Å, the (calculated) distance between the carbon atoms in 4-position of the pyridyl groups is significantly larger than in $[B_2(hpp)_2(L1)_2]^{2+}$ (exp. 5.1278(4) Å in the solid-state). The B–B–N angles (N being one of the pyridine-nitrogen atoms directly bound to boron) measure 125.2° and 125.3°, being significantly larger than the corresponding angles in $[B_2(hpp)_2(L1)_2]^{2+}$. In addition, the two pyridines in the (L1 + Me) units are twisted,

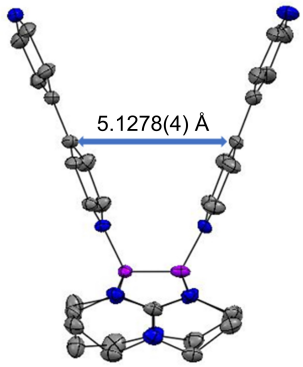

Figure 8. Illustration of the solid-state structure of $[B_2(hpp)_2(L1)_2]^{2+}$. Triflate counterions and hydrogen atoms omitted. Displacement ellipsoids drawn at the 50% probability level. Colour code: B purple, C grey, N blue.

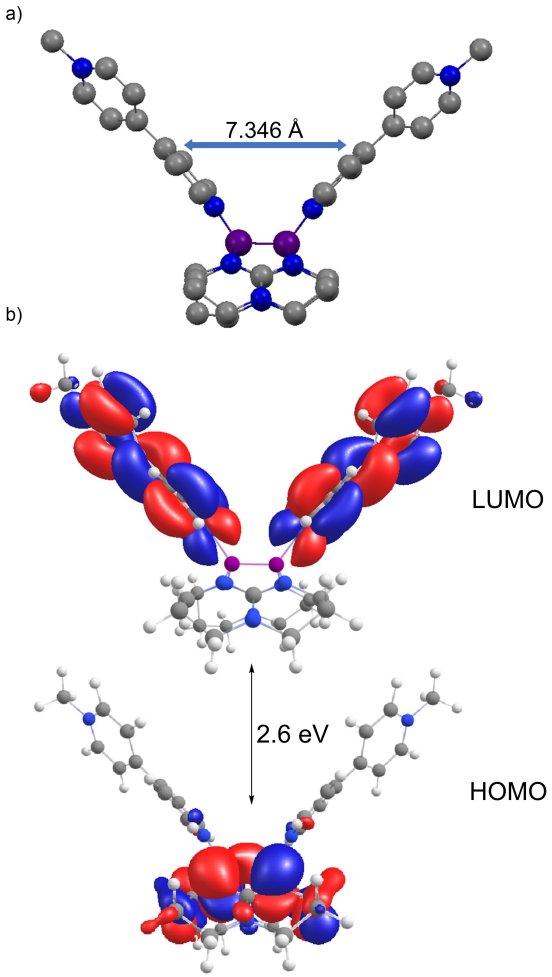

Figure 9. a) Visualization of the structure of $[B_2(hpp)_2(L1+Me)_2]^{4+}$ (hydrogen atoms omitted) from a B3LYP + D3/def2-TZVP calculation. Colour code: B purple, C grey, N blue. b) Illustration of the isodensity surfaces (isovalue = 0.02) for the HOMO und LUMO of $[B_2(hpp)_2(L1+Me)_2]^{4+}$.

with an angle of 36.21° and 36.14° between the two pyridyl planes, whereas this angle measures only 15.53° and 13.77° in $[B_2(hpp)_2(L1)_2]^{2+}$. With 1.765 Å, the B–B bond length is calculated to be larger in $[B_2(hpp)_2(L1+Me)_2]^{4+}$ than in $[B_2(hpp)_2(L1)_2]^{2+}$ (exp. 1.7005(1) Å). Similar to the cyclophanes $[\{B_2(hpp)_2\}_2(L1)_2]^{4+}$ and $[\{B_2(hpp)_2\}_2(L3)_2]^{4+}$, the HOMO is located exclusively on the diboron unit and the LUMO on the (L1 + Me) units (Figure 9b). The HOMO-LUMO gap of 2.6 eV is similar to that in $[\{B_2(hpp)_2\}_2(L1)_2]^{4+}$.

In Figure 10, the UV-vis spectra of the two open-structure compounds $[B_2(hpp)_2(L1)_2]^{2+}$ and $[B_2(hpp)_2(L1+Me)_2]^{4+}$ are compared with that of the cyclophane $[\{B_2(hpp)_2\}_2(L1)_2]^{4+}$. For $[B_2(hpp)_2(L1)_2]^{2+}$, a shoulder at 316 nm can be assigned to a charge-transfer excitation from the diboron unit to the bipyridyl units (Figure 10). The energy of the charge-transfer band decreases from 316 nm for $[B_2(hpp)_2(L1)_2]^{2+}$ to 361 nm for $[B_2(hpp)_2(L1+Me)_2]^{4+}$. Obviously, $(L1+Me)^+$ is a better electron acceptor than L1. The charge-transfer band of $[\{B_2(hpp)_2\}_2(L1)_2]^{4+}$ shows again at lower energy (397 nm). The larger extinction coefficient of the charge-transfer transition of $[\{B_2(hpp)_2\}_2(L1)_2]^{4+}$ is in line with the presence of two instead of only one diboron unit.

The cyclic voltammograms of the two open-structure compounds containing L1 or (L1 + Me) are shown in Figure 11. In Table 2 the potentials are compared to those of the cyclophane $[\{B_2(hpp)_2\}_2(L1)_2](OTf)_4$. The tetracation $[B_2(hpp)_2(L1+Me)_2]^{4+}$, with $E_{1/2} = -0.58$ V for the first redox process assigned to the redox couple $[B_2(hpp)_2(L1+Me)_2]^{4+}/[B_2(hpp)_2(L1+Me)_2]^{2+}$, is the strongest electron acceptor of the three compounds. In contrast to $[\{B_2(hpp)_2\}_2(L1)_2]^{4+}$, this two-electron reduction step is not split into two one-electron reduction steps, indicating the absence of significant electronic coupling between the two dicationic organic units in the tetracationic compound. This result could be explained by the large spatial separation of the two units. Further reduction is split into two one-electron events, with $E_{1/2}$ values of −1.06 V for the redox couple $[B_2(hpp)_2(L1+Me)_2]^{2+}/[B_2(hpp)_2(L1+Me)_2]^{+}$ and −1.15 V for $[B_2(hpp)_2(L1+Me)_2]^{+}/[B_2(hpp)_2(L1+Me)_2]^{0}$. Thus, electronic coupling is switched on after two-electron reduction, that

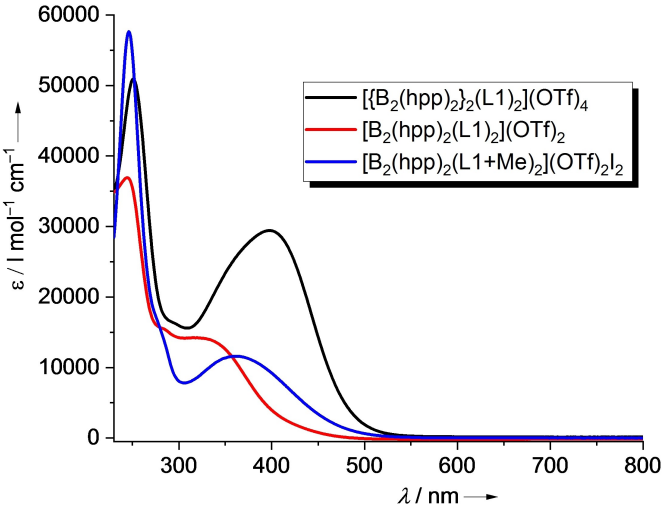

Figure 10. UV-vis spectra of $[\{B_2(hpp)_2\}_2(L1)_2](OTf)_4$ (black curve), $[B_2(hpp)_2(L1)_2](OTf)_2$ (red curve) and $[B_2(hpp)_2(L1+Me)_2](OTf)_2I_2$ (blue curve) in CH_3CN.

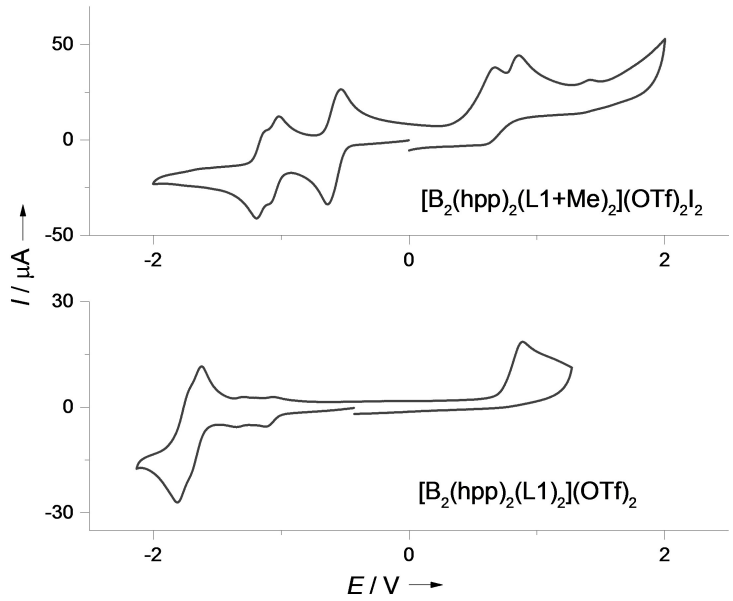

Figure 11. Comparison between the cyclic voltammograms for $[B_2(hpp)_2(L1+Me)_2](OTf)_2I_2$ and $[B_2(hpp)_2(L1)_2](OTf)_2$ in CH_3CN at 298 K, measured at a scan rate of 100 mV s^{-1} (glassy carbon working-electrode, Pt counter-electrode, Ag/AgCl reference-electrode, 0.1 M nBu_4NPF_6 as supporting electrolyte). Potentials are given vs. the ferrocenium/ferrocene (Fc^+/Fc) redox couple.

Table 2. Potentials (in V, given vs. Fc^+/Fc) measured in CH_3CN solution.

Compound	$E_{1/2}(1)/E_{red}(1)$	$E_{1/2}(2)/E_{red}(2)$	$E_{1/2}(3)/E_{red}(3)$	$E_{1/2}(4)/E_{red}(4)$
$[\{B_2(hpp)_2\}_2(L1)_2](OTf)_4$	−1.14/−1.18	−1.21/−1.38	−1.80/−1.87	−2.06/−2.10
$[B_2(hpp)_2(L1+Me)_2](OTf)_2I_2$	−0.58/−0.64	−0.58/−0.64	−1.06/−1.10 [a]	−1.15/−1.19 [a]
$[B_2(hpp)_2(L1)_2](OTf)_2$	−1.68/−1.74	−1.77/−1.81		

[a] Outside the available potential window in the solvent.

decreases the electronic repulsion between the two organic units and presumably decreases their spatial separation. Please note that irreversible oxidation of the iodide counter-ions is observed at quite high potential ($E_{ox} = +0.67$ V), in line with strong interactions between the iodide ions and the tetracations in CH_3CN solution. Another irreversible oxidation at $E_{ox} = +0.86$ V is tentatively assigned to oxidation of the diboron unit ($B^{II} \rightarrow B^{III}$) accompanied with decomposition. In the case of $[B_2(hpp)_2(L1)_2]^{2+}$, the reduced electron-acceptor character of the bipyridyl units leads to a significant shift of the redox potentials to lower values. Two one-electron processes with only slightly different potentials are visible, at −1.68 V for the redox couple $[B_2(hpp)_2(L1)_2]^{2+}/[B_2(hpp)_2(L1)_2]^+$, and at −1.77 V for $[B_2(hpp)_2(L1)_2]^+/[B_2(hpp)_2(L1)_2]$. The reduced electronic repulsion allows a smaller spatial separation between the bipyridyl units, initiating weak electronic coupling already before reduction. An irreversible oxidation at $E_{ox} = +0.89$ V is likely to belong to oxidation of the diboron unit ($B^{II} \rightarrow B^{III}$) accompanied with decomposition.

In addition to the dicationic open-structure compounds $[B_2(hpp)_2(L1)_2]^{2+}$ and $[B_2(hpp)_2(L2)_2]^{2+}$, we synthesized the dicationic diborane $[B_2(hpp)_2(L7)]^{2+}$, with a unit L7 also containing two uncoordinated nitrogen atoms. Reaction of **1** with 2,2′-bipyrimidine (L7) in CH_2Cl_2 solution at room temperature yielded the salt $[B_2(hpp)_2(L7)](OTf)_2$, that precipitated in 38% isolated yield in the form of orange crystals suitable for SCXRD from a CH_2Cl_2 solution layered with *n*-pentane (Figure 12). It was not possible to coordinate a second $[B_2(hpp)_2]^{2+}$ unit to L7, even not with a large excess of diborane **1**. Moreover, attempts to coordinate a transition metal (reactions with $Mn(CO)_5Br$, $Ru(bipy)_2Cl_2$, $[Rh(cod)Cl]_2$, and $W(CO)_6$) were fruitless. Obviously, the Lewis basicity of the two remaining uncoordinated N atoms is significantly reduced by the coordination of L7 to one diboron unit. Figure 12 visualizes the solid-state structure of the dication $[B_2(hpp)_2(L7)]^{2+}$.[24] The B–B bond length measures 1.670 Å, and the two B–N bonds connecting the diboron unit with the bipyrimidine unit measure 1.600 and 1.606 Å.

The cyclic voltammogram of $[B_2(hpp)_2(L7)](OTf)_2$ shows two (one-electron) redox processes at $E_{1/2}(1) = -0.96$ V and $E_{1/2}(2) = -1.52$ V (Figure 13). The Lewis structures on the right side sketch the overall, 2,2′-bipyrimidine-centered two-electron redox process. However, the reduction waves are more intense than the oxidation waves, arguing for partial loss of compound after the second reduction. Attempts to chemically reduce the compound with $CoCp^*_2$ resulted in product mixtures from which a clean product could not be isolated.

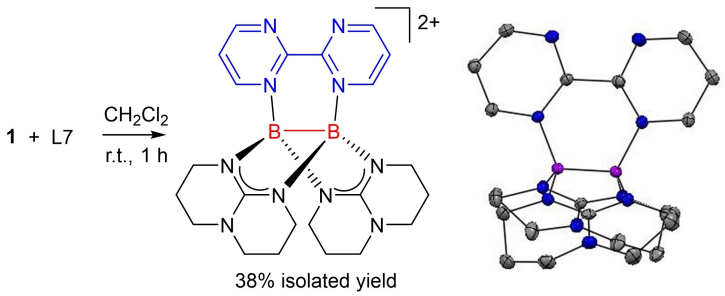

Figure 12. Synthesis of $[B_2(hpp)_2(L7)]^{2+}$ and illustration of the solid-state structure of $[B_2(hpp)_2(L7)]^{2+}$. Triflate counterions and hydrogen atoms omitted. Displacement ellipsoids drawn at the 50% probability level. Colour code: B purple, C grey, N blue.

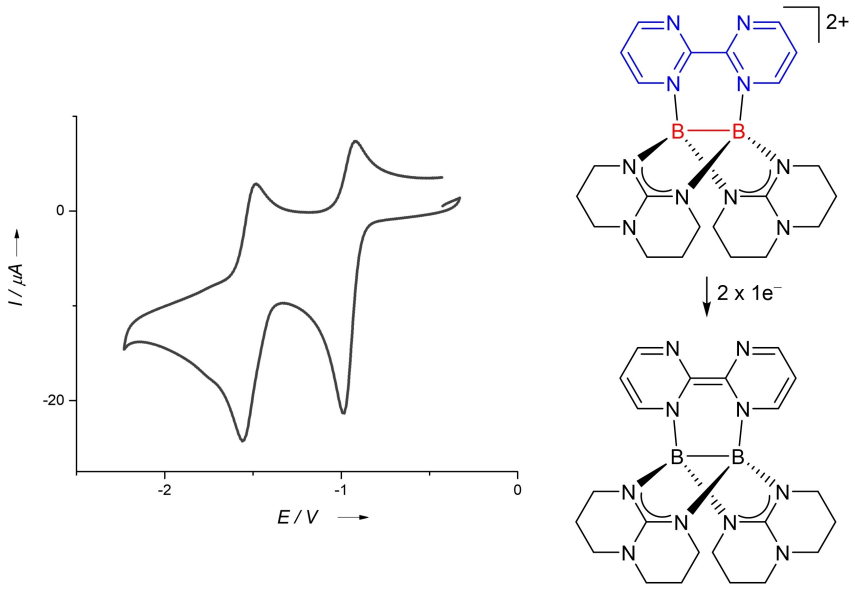

Figure 13. Cyclic voltammogram of a 1 mM solution of $[B_2(hpp)_2(L7)](OTf)_2$ in CH_3CN at 298 K, measured at a scan rate of 100 mV s^{-1} (glassy carbon working electrode, platinum counter electrode, Ag/AgCl reference electrode, 0.1 M nBu_4NPF_6 as supporting electrolyte). Potentials given vs. the ferrocenium/ferrocene (Fc^+/Fc) redox couple.

Construction of the first hexaboracyclophane cage

An important aim of this work was the construction of a first polycationic macrocycle with cage-like structure and integrated electron-rich diboron units. To demonstrate the possibility to synthesize such compounds with a charge higher than +4, we used the trispyridine compound tris(4-pyridyl)triazine (L8). To our delight, reaction of L8 with the diborane **1** yielded the unprecedented hexacationic hexaboron cage compound $[\{B_2(hpp)_2\}_3(L8)_2]^{6+}$ (Scheme 5), that crystallized together with six triflato counterions in the form of dark-red crystals in 38% isolated yield. Several experiments showed that the use of an excess of L8 has a positive impact on the yield. The red salt was barely soluble in CH_2Cl_2, but moderately soluble in CH_3CN. The ^{11}B NMR spectrum contained a single signal at $\delta = 4.08$ ppm, showing the equivalence of all six boron atoms. Also, in the ^1H NMR spectrum, only two doublets appeared in the aromatic region (at $\delta = 8.58$ and 8.30 ppm), in line with the chemical equivalence of all six pyridyl groups. Interestingly, here again the reaction mixture turned deep-green instantly upon dissolving the two reactants in CH_2Cl_2 (Scheme 5). After some time it changed colour to red, signaling formation of the final product. Following the conclusions drawn for other reactions (see discussion above), we postulate an intermediate in which only one of the triflates of the diborane reagent is substituted by L8 to be responsible for the dark-green colour.

The solid-state structure from SCXRD is shown in Figure 14 from two perspectives.[24] The three B–B bond lengths are only slightly different in the solid state, measuring 1.7259(1), 1.7213(1) and 1.7280(1) Å, in line with the presence of three intact B–B bonds. The B–N bonds, connecting the diboron units with the L8 units, are 1.5711(1)–1.5867(2) Å long. The shortest C···C distance between C atoms from different triazine units amounts to 3.8278(3) Å.

The UV-vis spectrum of $[\{B_2(hpp)_2\}_3(L8)_2](OTf)_6$ in CH_3CN solution (Figure 15a) shows a sharp band at 241 nm and a broad band centered at 391 nm, extending far into the visible region. The broad band is again assigned to a charge-transfer

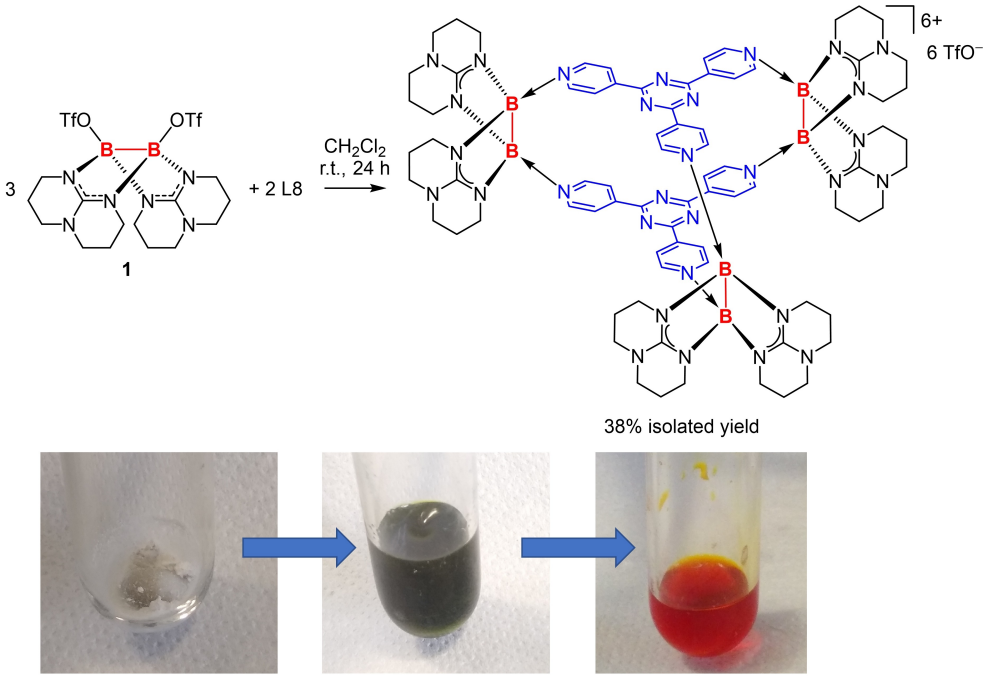

Scheme 5. Synthesis of the first hexacationic hexaboron cage $[\{B_2(hpp)_2\}_3(L8)_2](OTf)_6$ with three diboron units. The photos show (from left to right) the colorless mixture of the two reactants **1** and L8, the dark-green reaction mixture directly after addition of CH_2Cl_2, and a solution of the red final product $[\{B_2(hpp)_2\}_3(L8)_2](OTf)_6$ in CH_3CN.

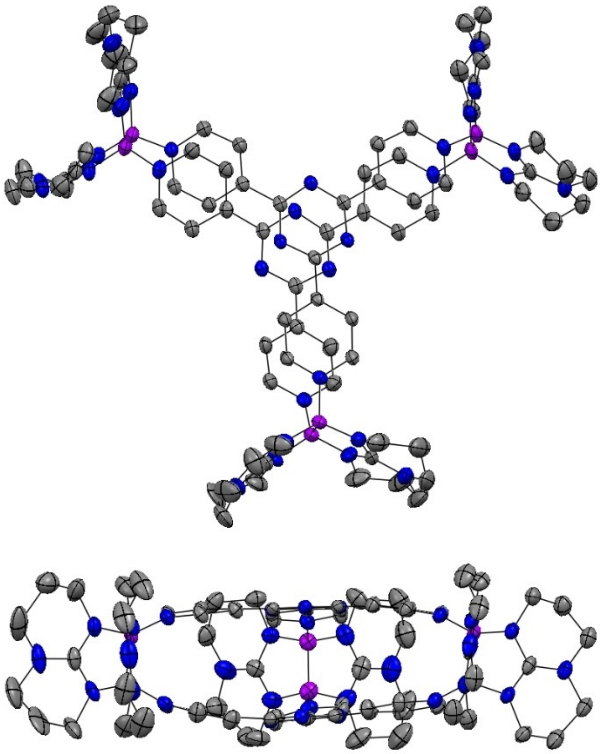

Figure 14. Illustration of the solid-state structure of $[\{B_2(hpp)_2\}_3(L8)_2]^{6+}$ from two perspectives. Triflate counterions and hydrogen atoms omitted. Displacement ellipsoids drawn at the 50% probability level. Colour code: B purple, C grey, N blue.

transition from an orbital localized on the electron-rich diboron units (HOMO) to an unoccupied orbital at the trispyridyl (L8) electron-acceptor units (LUMO). For comparison, the UV-vis spectrum of free L8 is dominated by a strong band at 245 nm; L8 does not absorb in the visible region.

Cyclic voltammetry measurements show that the hexacation $[\{B_2(hpp)_2\}_3(L8)_2]^{6+}$ can be reduced reversibly in five steps to the neutral compound (Figure 15b). On the basis of their relative intensities, we assign the waves to four one-electron and one two-electron redox events. The four reversible one-electron processes are observed at $E_{1/2} = -0.88$, -1.03, -1.51 and -1.68 V. Then a reversible two-electron redox process follows at $E_{1/2} = -2.07$ V. For comparison, free L8 exhibits a reduction wave at -1.73 V. The observation of one-electron redox processes indicates electronic communication between the two tris(4-pyridyl)triazine units, enabled by their small spatial separation. The possibility for reversible stepwise reduction with up to six electrons makes the new cage-like hexacation interesting for applications (e.g. as energy-storage material). The reduction potential for the redox couple $[\{B_2(hpp)_2\}_3(L8)_2]^{6+}$ /$[\{B_2(hpp)_2\}_3(L8)_2]^{5+}$ is quite high, motivating attempts to chemically reduce the compounds. Unfortunately, up to date all attempts to chemically reduce the hexacationic cyclophane and to isolate a product of reduction failed, although some redox experiments look promising. For example, reaction with two or four equivalents of $CoCp_2$ or $CoCp^*_2$ in CH_2Cl_2 led to a colour change from red to green, pointing to a change in redox state. However, the solution darkened after some time indicating conversion to other, so far unidentified products. Hence, we

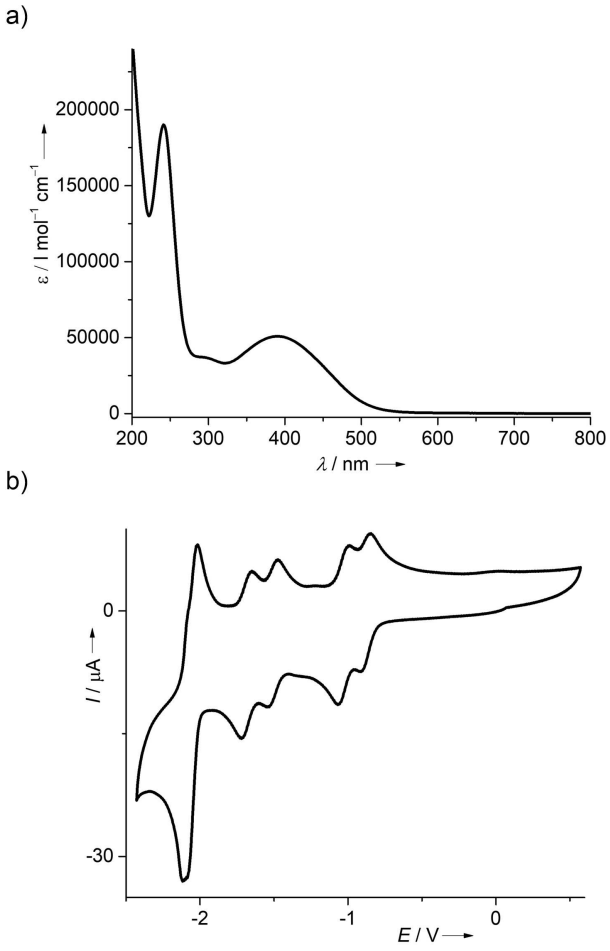

Figure 15. a) UV-vis spectrum of the new hexaboron cage $[\{B_2(hpp)_2\}_3(L8)_2](OTf)_6$ in CH_3CN. b) Cyclic voltammogram of $[\{B_2(hpp)_2\}_3(L8)_2](OTf)_6$ in CH_3CN at 298 K, measured at a scan rate of 100 mV s^{-1} (glassy carbon working-electrode, Pt counter-electrode, Ag/AgCl reference-electrode, 0.1 M nBu_4NPF_6 as supporting electrolyte). Potentials are given vs. the ferrocenium/ferrocene (Fc^+/Fc) redox couple.

could not yet confirm the stability of the compounds in several redox states.

Conclusions

This work is the first systematic study of polycationic cyclophanes and cage-like compounds built of bi- or tris-pyridyl electron-acceptor units and electron-rich diboron units. The synthesis of these novel compounds relies on an easily accessible, electron-rich ditriflato-diborane precursor with strongly electron-donating guanidinate groups, that allows the integration of electron-rich diboron electron-donor units in a variety of polycationic cyclophanes. An important result of this work is the synthesis of a first hexacationic cage-like compound, in which two tris(4-pyridyl)triazine electron-acceptor units are connected by three diboron units. Due to the presence of the diboron electron-donor units in combination with the bi- or oligopyridyl electron-acceptor units, the compounds display intriguing redox and optical properties, and the results demonstrate that these properties could be tuned in a rational way by the size and other properties of the viologen-like electron-acceptor units. Quantum-chemical calculations on selected compounds show that the HOMO is localized on the diboron units and the LUMO exclusively on the bispyridyl units, leading to characteristic charge-transfer excitations in the visible region.

We demonstrate in addition the possibility to synthesize open-structure compounds, in which two viologen-like units are connected by only one diboron unit. Such compounds might provide access to asymmetric rings and cages with only one diboron unit and a variable organic unit at the "other side" that binds to both bispyridyl units to close the ring.

Research on this novel class of compounds is still at its infancy. An important aim of ongoing research is the isolation and characterization of cyclophanes in different redox states. Another aim is the increase of the ring or cavity size. The diboron units permit only a small spatial separation between the aromatic systems in the cyclophanes with bi- or oligopyridyl linkers, too small for the uptake of an organic donor molecule. On the other hand, the increase of the electron-acceptor property by introduction of further electron-withdrawing substituents, for example at the phenylene ring of the L3 units in $[\{B_2(hpp)_2\}_3(L3)_2]^{4+}$, might trigger an intramolecular electron transfer (IET) from the B–B bond to the bispyridyl units. Similar IET processes were already observed for cyclophanes with pyrazine units (see Introduction and Scheme 2). The cleavage of the B–B bond in the course of this IET increases the size of the ring system, thereby possibly initiating the uptake of an aromatic guest molecule. Moreover, rings with larger diameter, able to receive organic guest molecules, could be realized in asymmetric compounds in which the two bispyridyl groups are connected by one diboron unit and an organic group of variable size at the other side. A suitable precursor to such compounds might be the open-structure compound $[B_2(hpp)_2(L1)_2]^{2+}$ reported in this work.

Acknowledgements

The authors gratefully acknowledge financial support by the German Research Foundation (DFG). Open Access funding enabled and organized by Projekt DEAL.

Conflict of Interest

The authors declare no conflict of interest.

Keywords: bispyridines · boron · cyclophanes · diborane · donor-acceptor compounds

[1] J. Ding, C. Zheng, L. Wang, C. Lu, B. Zhang, Y. Chen, M. Li, G. Zhai, X. Zhuang, *J. Mater. Chem. A* **2019**, *7*, 23337–23360.

[2] B. Odell, M. V. Reddington, A. M. Z. Slawin, N. Spencer, J. F. Stoddart, D. J. Williams, *Angew. Chem. Int. Ed.* **1988**, *27*, 1547–1550; *Angew. Chem.* **1988**, *100*, 1605–1608.
[3] M. Bühner, W. Geuder, W.-K. Gries, S. Hünig, M. Koch, T. Poll, *Angew. Chem. Int. Ed.* **1988**, *27*, 1553–1556; *Angew. Chem.* **1988**, *100*, 1611–1614.
[4] J. F. Stoddart, *Angew. Chem. Int. Ed.* **2017**, *56*, 11094–11125; *Angew. Chem.* **2017**, *129*, 11244–11277.
[5] P. R. Ashton, B. Odell, M. V. Reddington, A. M. Z. Slawin, J. F. Stoddart, D. J. Williams, *Angew. Chem. Int. Ed.* **1988**, *27*, 1550–1553; *Angew. Chem.* **1988**, *100*, 1608–1611.
[6] S. M. Dyar, J. C. Barnes, M. Juricek, J. F. Stoddart, D. T. Co, R. M. Young, M. R. Wasilewski, *Angew. Chem. Int. Ed.* **2014**, *53*, 5371–5375; *Angew. Chem.* **2014**, *126*, 5475–5479.
[7] Q.-H. Guo, J. Zhou, H. Mao, Y. Qiu, M. T. Nguyen, Y. Feng, J. Liang, D. Shen, P. Li, Z. Liu, M. R. Wasielewski, J. F. Stoddart, *J. Am. Chem. Soc.* **2020**, *142*, 5419–5428.
[8] O. Anamimoghadam, J. A. Cooper, M. T. Nguyen, Q. H. Guo, L. Mosca, I. Roy, J. Sun, C. L. Stern, L. Redfern, O. K. Farha, J. F. Stoddart, *Angew. Chem. Int. Ed.* **2019**, *58*, 13778–13783; *Angew. Chem.* **2019**, *131*, 13916–13921.
[9] P. Chen, F. Jäkle, *J. Am. Chem. Soc.* **2011**, *133*, 20142–20145.
[10] P. Chen, R. A. Lalancette, F. Jäkle, *Angew. Chem. Int. Ed.* **2012**, *51*, 7994–7998; *Angew. Chem.* **2012**, *124*, 8118–8122.
[11] P. Chen, X. D. Yin, N. Baser-Kirazli, F. Jäkle, *Angew. Chem. Int. Ed.* **2015**, *54*, 10768–10772; *Angew. Chem.* **2015**, *127*, 10918–10922.
[12] N. Baser-Kirazli, R. A. Lalancette, F. Jäkle, *Angew. Chem. Int. Ed.* **2020**, *59*, 8689–8697; *Angew. Chem.* **2020**, *132*, 8767–8775.
[13] N. Baser-Kirazli, R. A. Lalancette, F. Jäkle, *Organometallics* **2021**, *40*, 520–528.
[14] D. Shimoyama, N. Baser-Kirazli, R. A. Lalancette, F. Jäkle, *Angew. Chem. Int. Ed.* **2021**, *60*, 17942–17946.
[15] A. Widera, E. Filbeck, H. Wadepohl, E. Kaifer, H.-J. Himmel, *Chem. Eur. J.* **2020**, *26*, 3435–3440.
[16] A. Widera, H. Wadepohl, H.-J. Himmel, *Angew. Chem. Int. Ed.* **2019**, *58*, 5897–5901; *Angew. Chem.* **2019**, *131*, 5957–5961.
[17] A. Widera, E. Filbeck, H.-J. Himmel, *Eur. J. Inorg. Chem.* **2020**, 3017–3029.
[18] H.-J. Himmel, *Angew. Chem. Int. Ed.* **2019**, *58*, 11600–11617; *Angew. Chem.* **2019**, *131*, 11724–11742.
[19] A. Widera, D. Vogler, H. Wadepohl, E. Kaifer, H.-J. Himmel, *Angew. Chem. Int. Ed.* **2018**, *57*, 11456–11459; *Angew. Chem.* **2018**, *130*, 11627–11630.
[20] S. Litters, E. Kaifer, H.-J. Himmel, *Angew. Chem. Int. Ed.* **2016**, *55*, 4345–4347; *Angew. Chem.* **2016**, *128*, 4417–4420.
[21] S. Litters, E. Kaifer, H.-J. Himmel, *Eur. J. Inorg. Chem.* **2016**, 4090–4098.
[22] A. Widera, E. Kaifer, H. Wadepohl, H.-J. Himmel, *Chem. Eur. J.* **2018**, 24, 1209–1216.
[23] J. Horn, A. Widera, S. Litters, E. Kaifer, H.-J. Himmel, *Dalton Trans.* **2018**, *47*, 2009–2017.
[24] Deposition2095962 (for $[\{B_2(hpp)_2\}_2(L5)_2](OTf)_4 \cdot 2\ CH_2Cl_2$), 2095965 (for $[(hpp)_2B_2(L1)_2](OTf)_2 \cdot CH_2Cl_2$), 2095963 (for $[B_2(hpp)_2(L7)](OTf)_2 \cdot 3\ CH_2Cl_2$), 2095966 (for $[\{B_2(hpp)_2\}_2(L6)_2](OTf)_4 \cdot 2\ CH_2Cl_2$), 2095964 (for $\{[(hpp)_2B_2]_3(L8)_2\}(OTf)_6 \cdot CH_3CN$) and 2105833 (for $[\{B_2(hpp)_2\}_2(L3)_2](OTf)_4 \cdot 2\ CH_3CN$) contains the supplementary crystallographic data for this paper. These data are provided free of charge by the joint Cambridge Crystallographic Data Centre and Fachinformationszentrum Karlsruhe Access Structures service.
[25] T. P. Martyanov, E. N. Ushakov, V. N. Nuriev, N. A. Aleksandrova, S. K. Sazonov, A. I. Vedernikov, L. G. Kuz'mina, L. S. Klimenko, E. G. Martyanova, S. P. Gromov, *J. Org. Chem.* **2021**, *86*, 3164–3175.
[26] L. R. MacGillivray, J. L. Reid, J. A. Ripmeester, *J. Am. Chem. Soc.* **2000**, *122*, 7817–7818.
[27] G. Campillo-Alvarado, A. D. Brannan, D. C. Swenson, L. R. MacGillivray, *Org. Lett.* **2018**, *20*, 5490–5492.

Manuscript received: July 21, 2021
Accepted manuscript online: August 30, 2021
Version of record online: October 8, 2021

